Jurnal Mekanikal
Disember 2002, Bil. 14, 21 - 35

EFFECT OF SINGLE OVERLOAD ON STRESS DISTRIBUTION IN AN AXIALLY LOADED 2024-T351 ALUMINIUM ALLOY PLATE SPECIMEN WITH A HOLE

Prithvi Raj Arora[*1]
Tan Meng Lee[1]
A.M.S. Hamouda[2]
S.M. Sapuan[2]
ShahNor Basri[1]
Zairil Azhar Zaludin[1]

Department of Aerospace Engineering[1],
Department of Mechanical and Manufacturing Engineering[2],
Faculty of Engineering,
Universiti Putra Malaysia,
43400 UPM, Serdang
Selangor Darul Ehsan, Malaysia.

ABSTRACT

In the present investigation, overloading of 2024-T351 aluminium alloy plate of 6.40 mm thick with 6 mm diameter hole has been studied by means of a two-dimensional finite element (FE) analysis under plane stress condition. The material for the analysis is assumed to be isotropic, and von Mises failure criterion with linear isotropic hardening is incorporated. The residual stress fields around the hole edge have been obtained for an overload range of 33.9% to 99% of the yield stress. The results indicate that there exists a large amount of compressive tangential residual stress around the hole edge. Reverse yielding was observed for an overloading $\sigma_{OL} >$ *75% which is responsible for reducing the extent of compressive residual stresses around the hole edge. The elastic-plastic finite element analysis shows that there is a significant reduction of stress concentration factor with overloading. A model is also developed giving tangential residual stress at the hole edge for a given overload.*

Keywords: *finite element, overloading, hole, elastic and plastic stress concentrations, residual stresses, plasticity, stresses at hole edge, model*

1.0 INTRODUCTION

Failures at the edge of fastener holes have been extensively observed in aircraft components as well as other general machine parts. The load between mechanical components is usually transferred through the fasteners joints. The requisite amount of residual stress is introduced around the hole region by various techniques e.g. stress coining, cold working, overloading, surface rolling, low

[*]Corresponding author. Tel.: 603 – 8656 7125, Fax:603 - 8656 7099
E-mail address: prarora@yahoo.com (Prithvi Raj Arora)

plasticity burnishing, and laser shock peening, etc. [1-5] to avoid the premature failure and to enhance the fatigue life simultaneously. A single tensile overload can be used in combination with other methods to improve the fatigue life characteristics of the materials with stress raisers. A large number of experimental investigations [6-9] have been reported for long cracks in the literature indicating crack growth retardation including the crack arrest with a single tensile overload. The plastic zone size governs the residual stress field around the hole region and it depends on the overload applied to the specimen. Particularly very little information is available about the modelling of residual stresses due to overloading which can reduce the extent of experimental testing for getting meaningful data for design purposes.

In the present investigation a two-dimensional elastic-plastic finite element analysis (FEA) is carried out to assess the effect of pre-stressing/overloading on the stress distribution ahead of the hole in a 2024-T351 aluminium alloy plate specimen.

2.0 MATERIAL PROPERTIES AND METHODS

2.1 Material properties

A two-dimensional elastic-plastic finite element analysis is carried out using LUSAS-ANALYSTS [10] to study the effect of overloading on 2024-T351 aluminium alloy plate with a central hole. The plate specimen with 6.40mm thickness and 6mm diameter hole is subjected to various overloads. Each overload is of certain fraction of yield load corresponding to yield stress of the material. Upon unloading, the residual stresses are induced across the minimum section of the specimen i.e. from the hole edge to the external boundary of the specimen. The mechanical properties of 2024-T351 aluminium alloy in the rolling direction tested at Materials and Structures Laboratory of Aerospace Engineering Department, are given as follows:

Young's Modulus, E	71539 MPa
Yield strength, σ_y (0.2%)	421 MPa
Ultimate strength, σ_{ut} (True Stress)	633 MPa
Poisson's ratio, ν	0.28
Strain hardening exponent, n	0.156

The true stress-strain data points obtained from the test conducted (Figure 1) are used in the finite element analysis code to characterize the material behaviour. Stress Potential (Von Mises) material model is used in the elastic-plastic finite element analysis [10].

2.2 Model geometry and boundary conditions

The geometrical details of the 2024-T351-aluminium alloy plate specimen used for overloading are given in Figure 2. Only one quarter of the model is considered, being doubly symmetric about the centre of the specimen, for the analysis. To build the 2D model 8-noded isoparametric rectangular elements (QPM8) from LUSAS family of elements with 3×3 integration scheme are used. The analysis has been carried out under plane stress condition with thickness t and the stress behaviour around the hole is presumed to be independent of thickness [11]. The mesh is generated automatically in the model using 1725 QPM8 elements (Figure 3a) and an enlarged view around the hole region is given in Figure 3b. The nodes along the y-axis and x-axis are restrained to move in the x and y directions respectively along with the rotational constraint about the axis through the centre of the hole and perpendicular to the plane of the hole giving the boundary conditions for the present analysis.

2.3 Mechanics and details of overloading

The specimen is subjected to a uniform stress at the end of the specimen in the y-direction and the stress is calculated with respect to the actually applied load on the specimen. The stress applied, σ_{OL} is calculated as a fraction of the yield stress and is referred to as the overload in percentage of yield stress. Several overloading stresses, σ_{OL} have been applied to the specimen to check the incipient yielding at the hole edge, and this value of σ_{OL} has been observed to be approximately equal to 33.9% of yield stress. Further, the overloading stress σ_{OL} was selected in the range from 130 MPa to 440 MPa, corresponding to 33.9% to 105% of yield stress of the material, such that the stress at the hole edge should not exceed the ultimate strength of the material. A total of 29 overload cases have been considered for the present analysis. Automatic loading is used for loading phase, whereas the manual loading is used for the unloading phase for the finite element analysis due to the limitations of the LUSAS software.

3.0 RESULTS AND DISCUSSIONS

3.1 Stress field behaviour: Loading phase

For the loading phase the specimen was subjected to 10% overload and the theoretical stress concentration factor, the ratio of the tangential stress with the applied stress $\sigma_{\theta\theta}/\sigma$ at the edge of the hole, was determined to ensure the convergence and appropriateness of the meshing intensity around the hole edge. The computed stress concentration factor for an axial loading is observed to be approximately three, which compares well with the theoretical solution (Table 1) due to Kirsch [12], Heywood [13], and photo elastic results by Howland [14]. This elastic analysis validates the meshed model to be used for the present investigation.

At the overloading stress equal to or less than the incipient yielding value the tangential stress distribution around the hole resembles the elastic behaviour. As the amount of applied stress increases, the plastic zone around the hole edge spreads outwardly (Figure 4) represented by a horizontal plateau. The non-dimensional (ND) tangential stress, $\sigma_{\theta\theta}/\sigma_y$ increases with ND radial distance, r/R from the hole edge and reaches its maximum value and then reduces rapidly elastically with increase in ND radial distance. This trend continues until the applied stress reaches 80% overloading stress. Nevertheless, for extremely high overloading beyond 80% overloading stress the whole section yields giving the gross yield behaviour of the specimen beyond the hole edge. On the other hand, the ND-radial stresses are zero at the hole edge, increase rapidly with ND radial distance to a tensile peak value, and further decrease progressively with ND-radial distance (Figure 5). The maximum ND tensile radial stress is approximately 0.40 for an overloading value of 95%.

For the applied overloading in the range $33.9\% < \sigma_{OL} < 91\%$ the plastic stress concentration factor (SCF) decreases gradually from 3.08 to 1.34 (Figure 6). However, for the applied overloading in the range $91\% \leq \sigma_{OL} < 99\%$, the values of plastic SCF increases from 1.34 to 1.51. The present analysis is stopped for applied overloading $\sigma_{OL} = 99\%$ as explained in the preceding section.

3.2 Stress field behaviour: Unloading phase

The ND tangential residual stresses after unloading are shown in Figure 7 for applied overloading from 33.9% to 99%. The unloading causes redistribution of stresses away from the edge of the hole, giving residual stress distribution. During the loading phase for overloading more than 33.9% the spread of plastic region does depend on the extent of overloading. It is observed that the spread of plastic region is more for higher overload. The plastic flow is more extensive at the edge of the hole and less extensive as one goes away from the edge of the hole. This may be the region that the plastic stress concentration factor is less near the edge of the hole as compared to the location radially away from the hole edge. This increase in plastic stress concentration with ND radial distance leads to higher non-dimensional tangential stress with ND radial distance. As the influence of plastic deformation with the ND radial distance fades away the elastic region starts beyond this point and is given by immediate change in slope on the loading phase of the curve giving the ND elastic-plastic boundary/interface $r_{e\text{-}p}$. The ND tangential residual stresses are compressive near the hole edge, and they gradually become tensile in nature before the elastic plastic interface $r_{e\text{-}p}$ is reached, and remain completely of tensile in nature until the external boundary of the specimen is reached. It is also seen that the size of compressive stress region responsible for enhancing the life of a specimen/component during service loading depends primarily on the amount of overload subjected to the specimen material. The ND tangential residual stresses at elastic-plastic interface $r_{e\text{-}p}$ increases with applied overload (Figure 7). However, this ND tangential residual stress value at the elastic-plastic interface $r_{e\text{-}p}$ decreases for an applied overload

$\sigma_{OL} > 70\%$. This may be due to a very large value of $r_{e\text{-}p}$ and at that location of $r_{e\text{-}p}$ the stress concentration effect is very little being far away from the edge of the hole, hence a low value of ND tangential residual stress at the elastic-plastic interface $r_{e\text{-}p}$.

The ND radial residual stresses are equal to zero at the hole edge, but they decrease first with ND radial distance and then increase with further increase in ND radial distance from the hole edge (Figure 8). Nonetheless, this compressive behaviour of ND radial residual stresses alters to tensile nature afterwards with ND radial distance from the hole edge. Similar to ND tangential residual stresses, the magnitudes of ND radial residual stresses depend on the level of overloading.

3.3 Stresses at the hole edge

The trend of ND tangential residual stresses at the hole edge, corresponding to various overloading values in the range of 33.9%-99% for loading and unloading cases are summarised in Figure 9. As the overloading increases, the corresponding ND tangential residual stress $\sigma_{\theta\theta}/\sigma_y$ at the hole edge increases gradually from its tensile value of 1.02 for σ_{OL} equal to 33.9% and goes to its maximum tensile value 1.4735 for σ_{OL} equal to 100% (Figure 9) for the loading case. It is also observed that for $\sigma_{OL} \leq 91\%$ the ND tangential residual stress $\sigma_{\theta\theta}/\sigma_y$ increases linearly with applied σ_{OL} for the loading case. However, for $\sigma_{OL} > 90$ %, the ND tangential stress $\sigma_{\theta\theta}/\sigma_y$ increases with increase in the applied overload, σ_{OL}, at a faster rate, for the loading case.

For unloading case as the overloading increases, the corresponding ND tangential residual stress $\sigma_{\theta\theta}/\sigma_y$ at the hole edge increases gradually from zero for σ_{OL} equal to 33.9% to –1.49 for σ_{OL} equal to 99% (Figure 9). It is seen that the ND tangential residual stress at the hole edge increases linearly until $\sigma_{OL} = 75$ % for unloading case. For $75\% \leq \sigma_{OL} \leq 91$ %, ND tangential residual stress at the hole edge remains practically constant and then further increases beyond 91% overloading for unloading case. The reverse yielding is observed around the hole edge after the specimen is unloaded for the case of overload greater than 75%. An interesting phenomenon is that for $\sigma_{OL} > 75$ %, both the ND tangential stress curves for loading phase and ND tangential (residual) stress curves unloading phase appear to be mirror image of each other about abscissa being the plane of symmetry (Figure 9). This is a very important new phenomenon observed which needs further investigation. Conversely, the ND radial stresses at the hole edge, regardless of loading or unloading phase are always zero, which are not shown in the Figure 9.

3.4 Plastic region around the overloaded hole

The plastic strain is obtained by subtracting the elastic strain from the total strain corresponding to the stress in the plastic region. The plastic strain contours are obtained directly from the post processor facility of the LUSAS finite element software for the given load case of a particular overload subjected to the

specimen. The plastic strain contours for σ_{OL} of 75% are given in Figure 10. The mechanics of obtaining the elastic-plastic boundary/interface is explained in the preceding section. The yielding originating from the edge of the hole is also shown in Figure 10. The shape of plastic strain contours is approximately semi-elliptical. Hence, plastic strain region representing residual stress field around the fastener hole can be taken into account while building a model to assess the life of the component subjected to fatigue loading.

The spread of elastic-plastic boundary along the x-direction measured from the edge of the hole against the applied overload is given in Figure 11. Three distinct regions are shown in Figure 11. The region-I shows a linearly increasing ND elastic-plastic boundary $r_{e\text{-}p}/R$ from the hole edge for the range of overloading 33.9% to 85%. Whereas, in the region-II the value of ND elastic-plastic boundary $r_{e\text{-}p}/R$ remains practically constant at 1.34 with the overloading from 85% to 93%. The third region-III shows a high spurt in values with the overload beyond 93%. The analysis is carried out until an overload of 99% indicating the gross yielding of the specimen from the inner edge of the hole to the external boundary of the specimen. The 99% overload also corresponds to the stresses almost equal to the fracture stress at the inner edge of the hole.

3.5 Development of a model

The purpose of the model is to predict the ND tangential stress at the hole edge during the loading phase of the specimen as well as after unloading giving the residual ND tangential stress at the hole edge from the overload information. A model has been presented here to estimate the residual stresses for a given overloading on the specimen with a hole. Based on the finite element analysis results given in the preceding sections for the spread of plastic zone around the hole for a given overloading the location of the elastic-plastic boundary is obtained. The ND elastic-plastic boundary distance, $r_{e\text{-}p}/R$, is plotted against the overloading (Figure 11). The ND elastic-plastic boundary distance, $r_{e\text{-}p}/R$, versus overload data is represented by three different regions and is represented by the following equations:

Region – *I*: $33.9\% < \sigma_{OL} < 85\%$

$$\left(\frac{r_e - p}{R}\right) = 3.8091576 + 28.027067*\sigma_{OL} - 76.540245*\sigma_{OL}^{2} + 93.866372*\sigma_{OL}^{3} - 40.379729**\sigma_{OL}^{4} \quad (1)$$

Region – *II*: $85\% < \sigma_{OL} < 93\%$

$$\left(\frac{r_e - p}{R}\right) = 1.34 \quad (2)$$

Region – *III*: $93\% < \sigma_{OL} < 99\%$

$$\left(\frac{r_e - p}{R}\right) = -871011.87 + 3566328*\sigma_{OL} - 5475709.8*\sigma_{OL}^2 + 3736527.5*\sigma_{OL}^3 - 956127.04*\sigma_{OL}^4 \quad (3)$$

Also from the finite element analysis information gathered in the preceding sections the information about the stress at the hole edge for different overloads is collected and is presented in Figure 12 for loading and unloading cases. The ND tangential stress at the hole edge can be obtained from the ND elastic-plastic boundary, $r_{e\text{-}p}/R$, data for the loading and unloading cases using Figure 12.

4.0 CONCLUSIONS

The following conclusions are deduced from the finite element analysis of the overloading process:

1. The elastic-plastic finite element analysis shows that there is a significant reduction of stress concentration factor with overloading.
2. The results indicate that large compressive tangential residual stresses are induced at the hole edge upon unloading. Reverse yielding is observed for an overloading $\sigma_{OL} > 75\%$, which is responsible for reducing the extent of compressive residual stress during unloading.
3. A model is developed giving tangential residual stresses at the hole edge for a given overloading.

ACKNOWLEDGEMENT

The authors gratefully acknowledge the financial support of Ministry of Science, Technology & Environment, Malaysia (IRPA Project No.03-02-04-0089), for the provision of a research grant for this work

.

REFERENCES

1. Speakman, E. R., 1970, "*Fatigue life improvement through stress coining methods*", Achievement of High Fatigue Resistance in Metals and Alloys, ASTM STP 467, American Society of Testing and Materials, Philadelphia, Pa., pp 209-227.
2. Phillips, J. L., 1974, "*Sleeve cold working fastener holes*", AFML-TR-74-10, Vol. I, Air force Materials Laboratory, Wright –Patterson AFB, OH.

3. Nawwar, A. M. and Shewchuk, J., Dec.1983, "*The effect of preload on fatigue strength of residually stressed specimens*", Experimental Mechanics, pp 409-413.
4. Smith, P. R. and Shepard, M. J., 2000, "*Effect of laser shock processing power density and shot repetition on residual stress distribution and % cold work in Ti-6Al-4V*", Proc. 5th National Turbine Engine HCF Conference.
5. Prevey, P. S., 2001, "*The effect of low plasticity burnishing on the HCF performance and FOD resistance of Ti-6Al-4V*", Proc. 6th National Turbine Engine HCF Conference, Jacksonville, FL, Mar 5-8.
6. Damri, D. and Knott, J. F., 1991, "*Transient retardations in fatigue crack growth following a single peak overload*", Fatigue Fracture Engng. Mater. Struct., Vol.14, pp 709-719.
7. Bray, G.H., Reynolds, A. P., and Starke, E. A., Jr., 1992, "*Mechanisms of fatigue crack retardation following single tensile overloads in powder metallurgy aluminium alloys*", Metall. Trans., Vol. 23A, pp 3055-3066.
8. Lu, Y. and Li, K., 1993, "*A new model for fatigue crack growth after a single overload*", Engng. Fract. Mech., Vol. 46, pp 849-856.
9. Zhang, J. Z., Halliday, M. D., Bowen, P. and Poole, P., 1999, "*Three dimensional elastic-plastic finite element modelling of small fatigue crack growth under a single tensile overload*", Engng. Fract. Mech., Vol. 63, pp 229-251.
10. *LUSAS* (London University Stress Analysis System), 2001, FEA Ltd Forge House, 66 High Street, Kingston upon Thames, Surrey, KT1 1HN, United Kingdom.
11. Timoshenko, S. P. and Goodier, J. N., 1982, "*Theory of Elasticity*", McGraw-Hill, pp 15-16.
12. Kirsch, G., 1898, *VDI*, Vol. 42.
13. Heywood, R. B., 1952, "*Designing by Photoelasticity*", Chapman & Hall, Ltd., London.
14. Howland, R. J. C., 1930, Transactions of Royal Society (London), Series A, Vol. 229, pp 49.

Table 1 Comparison of stress concentration factors.

	Stress Concentration Factors	
	K_{tg}	K_{tn}
Kirsch	3.000	2.640
Heywood	3.047	2.681
Howland	3.043	2.682
FEM (LUSAS)	3.078	2.709

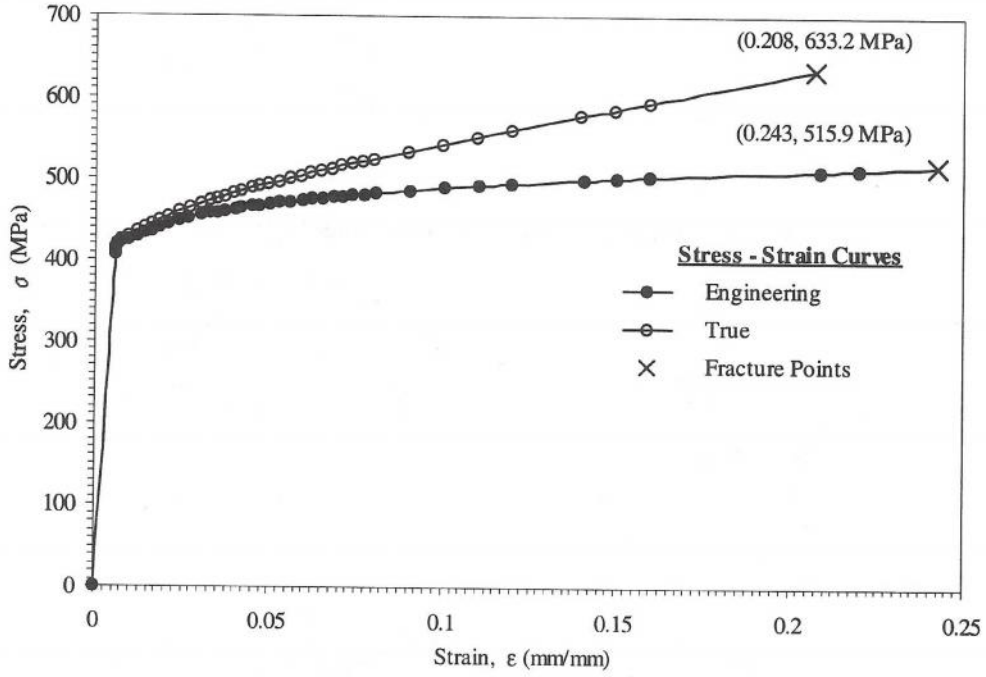

Figure 1 True stress-strain behaviour of 2024-T351 aluminium alloy

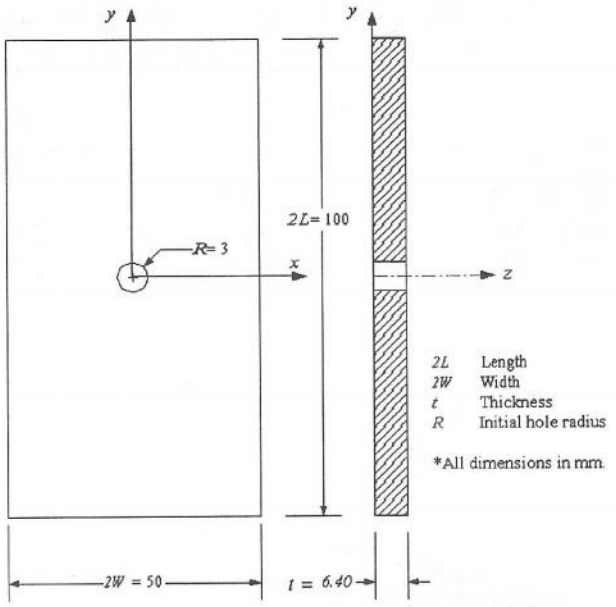

Figure 2 Geometrical details of the model specimen

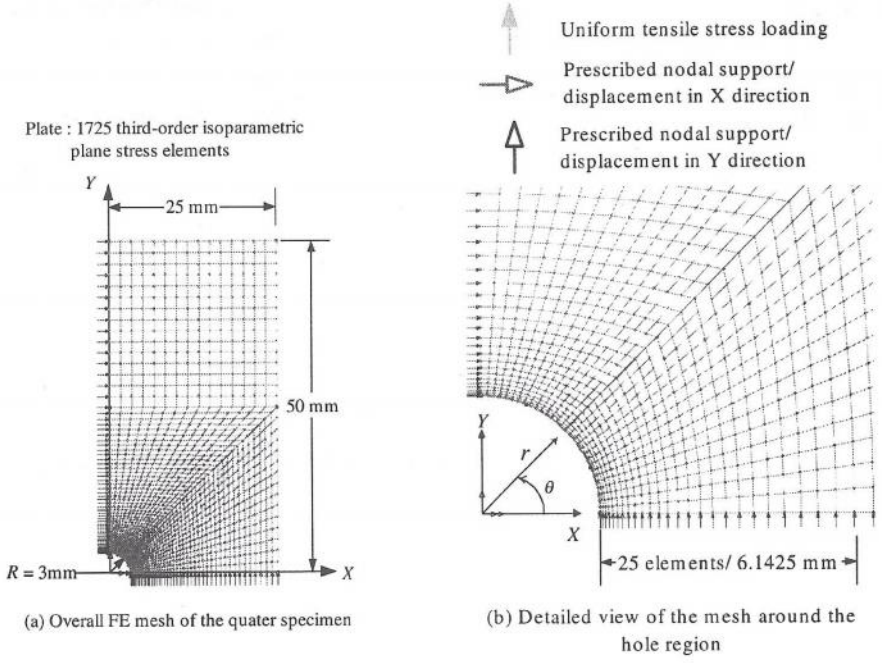

(a) Overall FE mesh of the quater specimen

(b) Detailed view of the mesh around the hole region

Figure 3 Two-dimensional FE model with uniform radial pressure loading

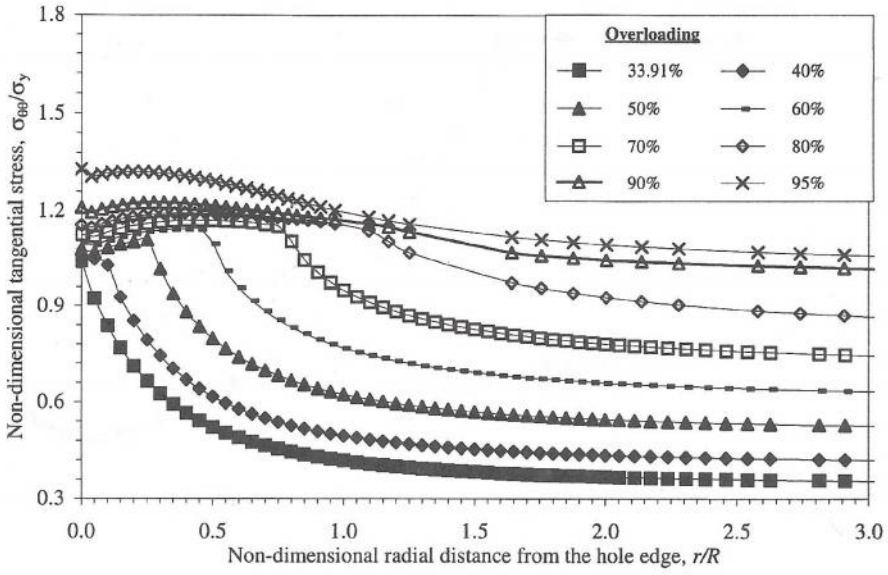

Figure 4 Non-dimensional tangential stress versus non-dimensional radial distance for the loading phase

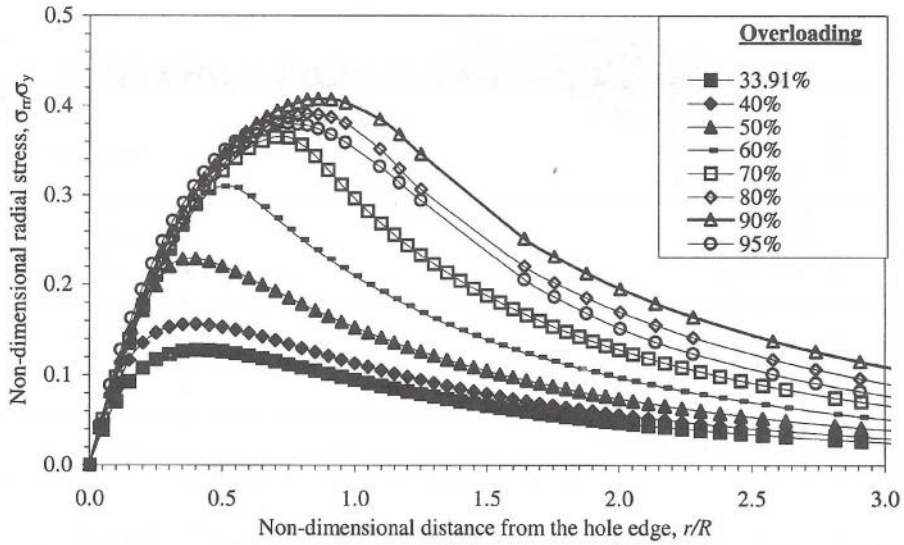

Figure 5 Non-dimensional radial stress versus non-dimensional radial distance for the loading phase

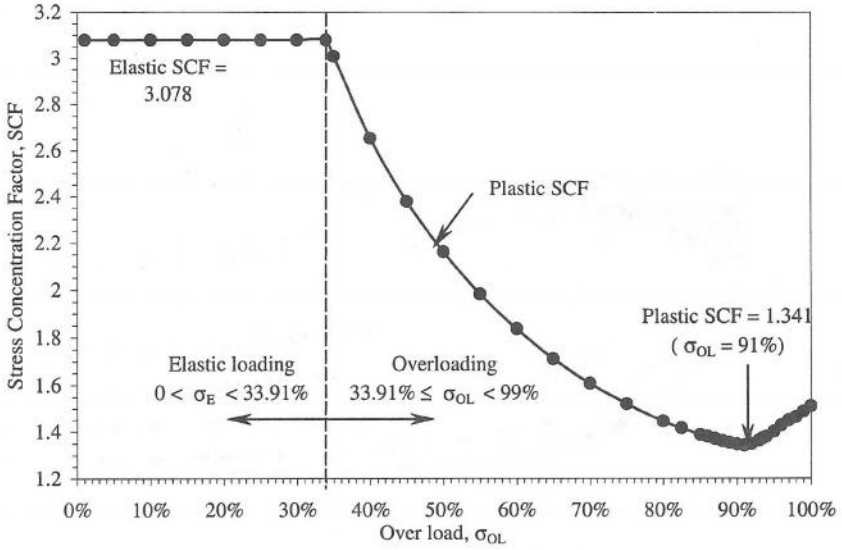

Figure 6 Stress concentration factor versus overload

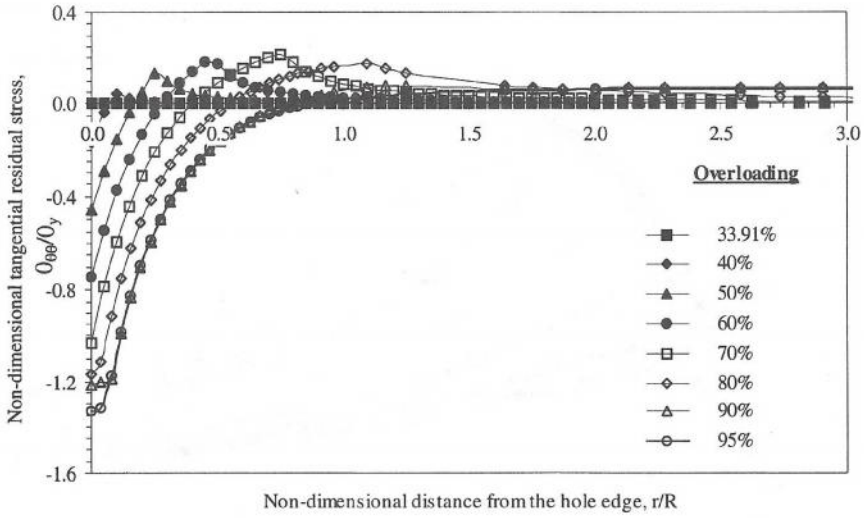

Figure 7 Non-dimensional tangential residual stress versus non-dimensional radial distance for the unloading phase

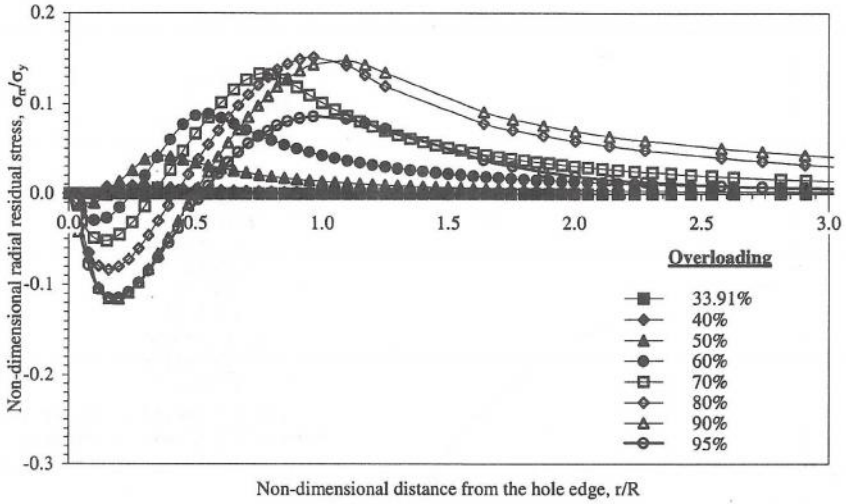

Figure 8 Non-dimensional radial residual stress versus non-dimensional radial distance for unloading phase

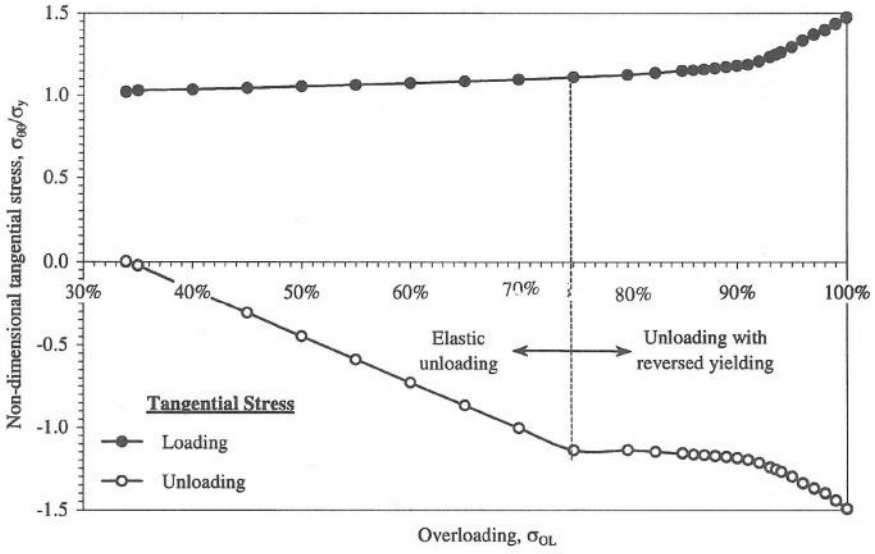

Figure 9 Non-dimensional tangential stress at hole edge versus applied tensile overloading stress (Note: Unloading representative of residual stresses)

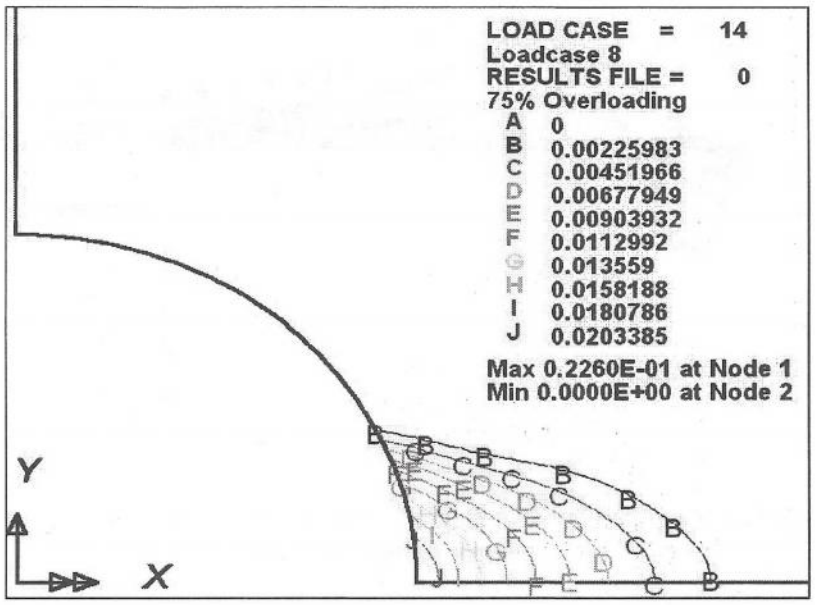

Figure 10 Contour plot of plastic region of 75% overloaded hole

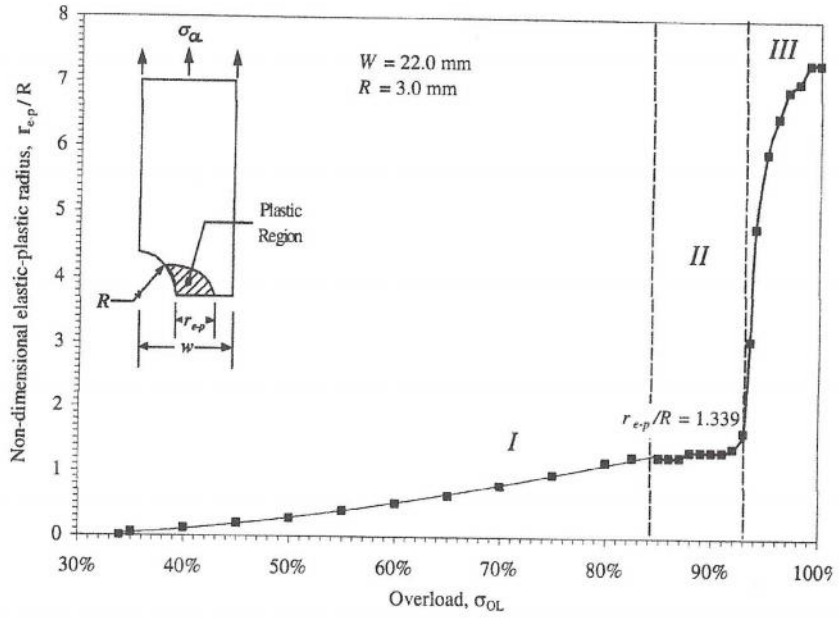

Figure 11 Non-dimensional elastic-plastic boundary versus tensile overloading

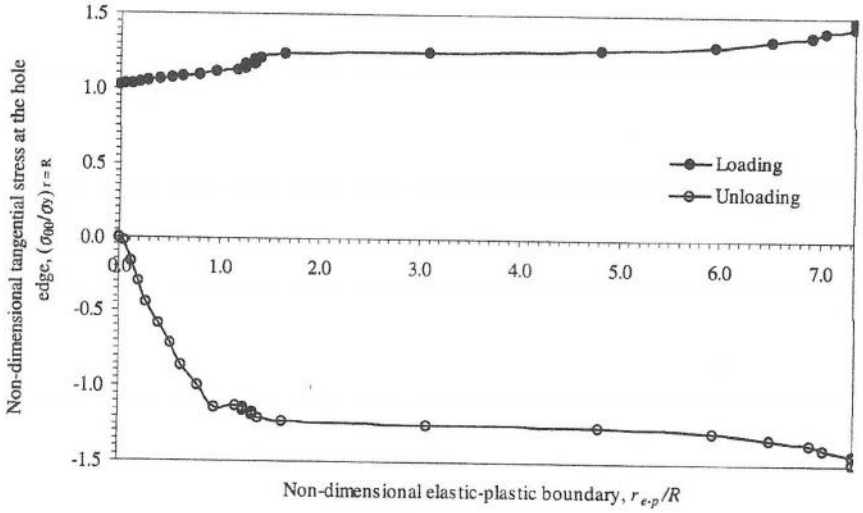

Figure 12 Non-dimensional tangential stress versus non-dimensional elastic-plastic boundary